Catalytic Function and Local Proton Structure at the Type 2 Copper of Nitrite Reductase: The Correlation of Enzymatic pH Dependence, Conserved Residues, and Proton Hyperfine Structure†

Yiwei Zhao,‡ Dmitriy A. Lukoyanov,‡,§ Yuriy V. Toropov,‡,|| Kenneth Wu,⊥ James P. Shapleigh,⊥ and Charles P. Scholes*,‡

Department of Chemistry, Center for Biophysics and Biochemistry, University at Albany, SUNY, Albany, New York 12222, and Department of Microbiology, Wing Hall, Cornell University, Ithaca, New York 14853

Received February 4, 2002; Revised Manuscript Received April 17, 2002

ABSTRACT: Electron nuclear double resonance (ENDOR) of protons at Type 2 and Type 1 cupric active sites correlates with the enzymatic pH dependence, the mutation of nearby conserved, nonligating residues, and electron transfer in heterologously expressed *Rhodobacter sphaeroides* nitrite reductase. Wild-type enzyme showed a pH 6 activity maximum but no kinetic deuterium isotope effect, suggesting protons are not transferred in the rate-limiting step of nitrite reduction. However, protonatable Asp129 and His287, both located near the Type 2 center, modulated enzyme activity. ENDOR of the wild-type Type 2 center at pH 6.0 revealed an exchangeable proton with large hyperfine coupling. Dipolar distance estimates indicated that this proton was 2.50−2.75 or 2.25−2.45 Å from Type 2 copper in the presence or absence of nitrite, respectively. This proton may provide a properly oriented hydrogen bond to enhance water formation upon nitrite reduction. This proton was eliminated at pH 5.0 and showed a diminished coupling at pH 7.5. Mutations of Asp129 and His287 reduced enzyme activity and altered the exchangeable proton hyperfine spectra. Mutation of Asp129 prevented a pH-dependent change at the Type 1 Cys167 ligand as observed by Cys C_β proton ENDOR, implying there is a Type 2 and pH-dependent alteration of the Type 1 center. Mutation of the Type 1 center ligand Met182 to Thr and mutation of Asp129 increased the activation energy for nitrite reduction. Involvement of both the Type 1 center and Asp129 in modulating activation energy shows that electron transfer from the Type 1 center to a nitrite-ligated Type 2 center is rate-limiting for nitrite reduction. Mutation of Ile289 to Ala and Val caused minor perturbation to enzyme activity, but as detected by ENDOR, allowed formate binding. Thus, bulky Ile289 may exclude non-nitrite ligands from the Type 2 active site.

The defining reaction of denitrification, unique to the denitrification process and catalyzed by nitrite reductase (Nir),[1] is the one-electron reduction of nitrite to nitric oxide. The formal reaction is

$$NO_2^- + 2H^+ + e^- \rightarrow NO + H_2O \qquad (1)$$

Copper-containing nitrite reductase (Nir) holds an unusual blue−green Type 1 copper center with a redox/electron-transfer function and at 12 Å distance a Type 2 copper center where nitrite binds and is reduced to nitric oxide. X-ray crystallographic structures of copper-containing Nir from *Achromobacter cycloclastes* (*1, 2*) and *Alcaligenes faecalis* (*3, 4*) have been reported with the Type 2 center in either oxidized (cupric) or reduced (cuprous) form and with that center either in the presence or in the absence of nitrite substrate. Although the above stoichiometric equation (eq 1) shows that there are transfers of an electron and of protons to nitrite substrate, the kinetic details of proton and electron transfer and their complementary relation to the intimate electronic and local proton hydrogen bond structure at the Type 2 center remain precisely to be determined.

Nir enzyme for our kinetic and spectroscopic study was obtained from a high-yield, heterologous *Escherichia coli* expression system derived from a denitrifying variant of *Rhodobacter sphaeroides* (*5*). Figure 1 provides a schematic of the locale of the Type 1 and Type 2 centers including

† These studies were partially supported by the NIH (GM-35103, C.P.S.) and the DOE (95ER20206, J.P.S.).

* To whom correspondence should be addressed at the Department of Chemistry, University at Albany, SUNY, Albany, NY 12222. Phone: 518-442-4551; Fax: 518-442-3462; E-mail: CPS14@albany.edu.

‡ University at Albany, SUNY.

§ On leave from the MRS Laboratory, Kazan State University, 420008, Kazan, Russian Federation.

|| Present address: Department of Physics, University of Wisconsin, 1150 University Ave., 2531 Stirling Hall, Madison, WI 53706-1390.

⊥ Cornell University.

[1] Abbreviations: RF, radio frequency; ptp, peak-to-peak; G, Gauss; i.d., inside diameter; o.d., outside diameter; EPR, electron paramagnetic resonance; ν_e, EPR frequency; ν_H, free proton NMR frequency; ENDOR, electron nuclear double resonance; Nir, nitrite reductase; WT, wild-type Nir; M182T, a mutant form of Nir where the Met182 residue at the Type 1 center was mutated to threonine; H287E, a mutant form of Nir where the His287 residue was mutated to glutamic acid; H287A, a mutant form of Nir where the His287 residue was mutated to alanine; D129A, a mutant form of Nir where the Asp129 was mutated to alanine; D129N, a mutant form of Nir where the Asp129 was mutated to asparagine; I289A, a mutant form of Nir where the Ile289 residue was mutated to alanine; I289V, a mutant form of Nir where the Ile289 residue was mutated to valine; iso-1-cyt *c*, yeast iso-1-cytochrome *c*; iso-1-ferrocyt *c*, yeast iso-1-ferrocytochrome *c*.

10.1021/bi0256274 CCC: $22.00
Published on Web 05/10/2002

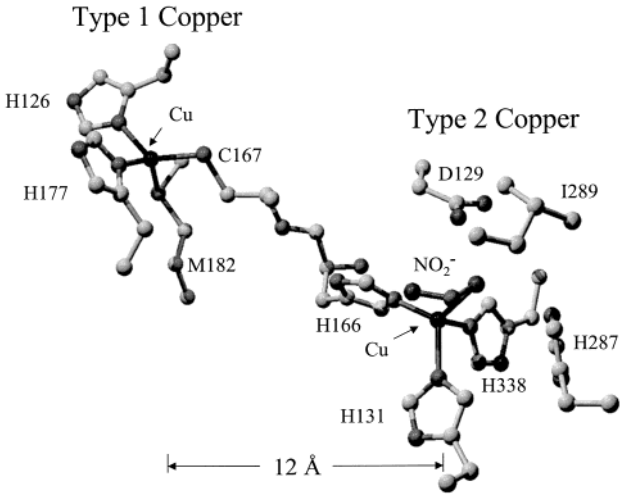

FIGURE 1: This figure shows the locale of the Type 1 blue−green electron-transfer center and the Type 2 catalytic center in nitrite reductase. The Type 1 and Type 2 copper centers are only ~12 Å apart and separated by His166 and Cys167. As ligands, Type 1 copper has His126, His177, Cys167, and Met182. As ligands, Type 2 copper has His166, His131, and His338, and an axial ligand which is nitrite or, in the absence of nitrite, either water or hydroxide. We also show conserved amino acids Asp129, His287, and Ile289 near the Type 2 catalytic center, whose roles we have probed in this study. [Structure after Murphy et al. (*4*), PDB file 1AS6, but with the amino acids given *R. sphaeroides* labels. For *A. faecalis*, the amino acids His95, His145, Cys136, and Met150 at the Type 1 center respectively correspond to His126, His177, Cys167, and Met182 of *R. sphaeroides*; for *A. faecalis*, the amino acids His100, His135, His306, Asp98, His255, and Ile257 at the Type 2 center respectively correspond to His131, His166, His338, Asp129, His287, and Ile289 of *R. sphaeroides*].

metal, substrate, ligands, and nearby conserved but nonligating amino acids. This schematic was adapted from the *A. faecalis* Nir structure (*4*) but is given the residue numbering relevant to the *R. sphaeroides* enzyme. In our previous study (*5*), wild-type Nir was initially characterized by its blue−green Type 1 copper having rhombic EPR character, by a 247 mV midpoint potential, and by its nitrite reductase activity. Two significant mutant forms, one at the Type 1 center and the other at the Type 2 center, were studied: The one at the Type 1 center had the axial methionine mutated to threonine (M182T), and the result was a blue center, rather than a blue−green center, with a midpoint potential about 100 mV above the wild-type Type 1 center and a moderately diminished steady-state and limited turnover activity compared to wild-type enzyme. The other was a mutant near the Type 2 center and had a conserved but nonligating amino acid (His287) changed to glutamic acid (H287E); its functional result was greatly diminished activity. We then surveyed at pH 7.2 the ligating environment of both Type 1 and Type 2 cupric centers by ENDOR (*6*). For the Type 1 center, hyperfine couplings from the two histidine nitrogens of the blue−green Type 1 center [sometimes called a "perturbed" Type 1 center (*7*)] indicated a larger percentage nitrogen electron spin density difference from each other than found in other blue copper proteins, while the cysteine C_β proton hyperfine couplings showed a smaller pπ covalent electron spin density on their adjacent cysteine sulfur than found in other blue copper proteins (*8*). For the Type 2 catalytic center, there were exchangeable, dipolar-coupled proton ENDOR features as measured at pH 7.2 from an axial water or OH^- proton. The presence of nitrite substrate changed both the histidine nitrogen ligand hyperfine couplings and the coupling to nearby exchangeable proton features. Even though ligation of nitrite perturbs the EPR signal and the proton and histidine ligand nitrogen ENDOR of the Type 2 center, the ligation of nitrite to Type 2 copper through nitrite oxygens (*4*) provided no detectable hyperfine coupling to the nitrogen itself of the nitrite. The highly inactive Type 2 H287E mutant showed no evidence of perturbation to its proton hyperfine structure when nitrite was present.

Since our initial work, it has become obvious that the Nir mechanism requires an understanding of the role of residues beyond the immediate nearest-neighbor ligands, particularly at the Type 2 catalytic center. The pH dependence of the reaction (*9*−*11*) points to a role for residues beyond the immediate nearest copper ligands. Near the active site there exist conserved, protonatable Asp (Asp129 here) and His (His287 here), and mutation of either of these markedly reduces activity (*10*). X-ray information points to an interconnected hydrogen-bonded net that connects the conserved Asp and His to a series of internal waters and to the Type 2 substrate ligation site (*4*, *12*). There is also a conserved Ile (see sequence alignment, Figure 1S, Supporting Information) which is Ile289 here, whose bulky side chain occludes the ligand binding pocket but whose function is not clear.

Our initial coupled functional (*5*) and ENDOR spectroscopic approach (*6*) provided the background and the strategy for the present complementary kinetic and spectroscopic ENDOR studies which we now aim toward a more critical understanding of the intimate nitrite reductase mechanism. Our present focus is on understanding the kinetic mechanism of nitrite reduction and correlating our findings with structural insights from ENDOR. Our kinetic work has centered on the distinct pH dependence to the enzymatic activity and on its activation energy. ENDOR provides concomitant information on the existence of and distance to exchangeable protons near metal active sites, and ENDOR is required to resolve protons which are not resolved by protein X-ray crystallography.

EXPERIMENTAL PROCEDURES

Materials

DNA purification kits to isolate plasmid DNA, PCR products, or DNA from electrophoresis gels were used according to the manufacturer's specifications (Qiagen). DNA sequencing was performed using the ABI Prism Big Dye terminator cycle sequencing ready reaction kits according to the manufacturer's specifications (PE Biosystems) and analyzed using an Applied Biosystems 373 DNA sequencing system.

Mutant Development. D129A, D129N, H287A, I289A, and I289V mutants were developed by methods using two rounds of PCR. The explicit details of mutant development are given in the Supporting Information.

Protein Expression. Overexpression and purification of wild-type Nir and its mutants using the plasmid pET17b-*nirK* which contains ampicillin resistance and the Nir gene were carried out as described by Olesen et al. (*5*). SDS−PAGE analyses were performed to monitor the purification procedure. Protein concentration was determined by the Bradford assay (*13*) or by the Microprotein-PR kit from

Sigma. Copper content was measured by the 2,2′-biquinoline assay carried out on reduced protein (*14*). The content of copper is given (Table 1S, Supporting Information) in terms of copper per subunit of Nir, where each trimer of Nir contains three subunits. Samples for ENDOR measurements were concentrated by Microcon concentrators. Q-band samples of approximately 50 μL volume and approximate total copper concentration of 500 μM were contained within precision 2.0 mm i.d., 2.4 mm o.d. sample tubes (Vitrodynamics, Rahway, NJ). Deuterated samples were prepared by several exchanges of protein into the appropriate deuterated buffer using a Centricon concentrator.

For the present work, we used as reductant a form of recombinant yeast iso-1-cytochrome *c* (iso-1-cyt *c*) that we heterologously overexpressed in *E. coli* (*15*); this form has its C-terminal Cys102 converted to Thr102 (*16*). The C102T mutant of yeast iso-1-cyt *c* is functional even in vivo for yeast, and it does not have the problem of disulfide dimerization (*17*). A description of the growth and purification of this recombinant cytochrome *c* is given by DeWeerd et al. (*18*). The iso-1-cyt *c* was reduced with ascorbate and the ascorbate removed by a PD-10 column (Pharmacia). The concentration of iso-1-ferrocytochrome *c* (iso-1-ferrocyt *c*) was measured from its extinction of $\epsilon_{(\mathrm{Red})\ 550} = 3 \times 10^4\ \mathrm{M}^{-1}\ \mathrm{cm}^{-1}$.

Rationale for Using Reduction of Iso-1-ferrocytochrome c To Follow Nir Kinetics. Our experimental goal was to obtain limited-turnover initial rate information to correlate with ENDOR information as obtained from the very same Nir. The heterologous Nir overexpression system provided large quantities of genetically manipulatable protein needed for ENDOR and kinetic studies. There was also a need for large quantities of reductant with a physiologically appropriate redox potential in the 250 mV range. This was provided by iso-1-cyt *c* whose redox potential is in the appropriate physiological range [273 mV (*17*, *19*)] and is comparable to that of the Nir Type 1 center. There is minimal pH dependence to the redox potential of yeast iso-1-cyt *c* over the pH 5−7.5 range (*20*, *21*), and its consumption is readily monitored spectrophotometrically. We found that we obtained considerably better and reproducible activity using our iso-1-cyt *c* than we did with commercially available beef heart cytochrome. We point out that for the *R. sphaeroides* Nir under study, the precise electron donor is unknown but has been suggested to be a *c*-type cytochrome (*22*). There are no obvious electron donors encoded in the region of the chromosome containing *nirK* in *R. sphaeroides*, nor does a genome analysis reveal a cytochrome *c* that would likely be the electron donor. We note that a fast electron-transfer process from cytochrome c_{551} to copper-containing nitrite reductase of *A. xylosoxidans* has been reported (*23*). Cytochrome c_2 of *R. sphaeroides* was provided to us as a kind gift by M. Okamura, but this cytochrome, which interacts with photosynthetic bacterial reaction centers from *R. sphaeroides* (*24*), was not efficiently oxidized in the presence of *R. sphaeroides* Nir and nitrite. Our activity measurements with iso-1-ferrocyt *c* reductant showed both a pH dependence which is similar to that obtained with other unrelated, nonphysiolgical viologen reductants and an activation energy which indicates electron transfer between Type 1 and Type 2 centers. The implication of the pH dependence and the activation energy information is that the oxidation of iso-1-ferrocyt *c* reductant in the presence of Nir and nitrite reflects a rate-limiting process internal to Nir rather than electron transfer between the cytochrome and Nir. As judged from the findings, iso-1-cyt *c* was a reductant with a physiologically appropriate redox potential that *worked* to report the catalytic, rate-limiting events of our Nir samples.

Methods

Enzyme Assay. The activity of nitrite reductase was assayed in a semiquantiative fashion with the methyl viologen assay (*25*) whereby the total consumption of nitrite at pH 6 in the presence of Nir, methyl violgen, and dithionite was determined at the end of a set 20 min period by use of the Griess reagent. Details of the method are given in the Supporting Information. This is a useful method for assaying mutants with very low activity.

Kinetic Measurements. Stopped-flow kinetic measurements were performed with a Aminco-Morrow stopped-flow attachment coupled to a retrofitted DW-2 UV−Vis spectrophotometer [the original by SLM Instruments, Urbana, IL, retrofitted by On Line Instrument Systems (OLIS), Inc., Jefferson, GA]. Kinetic data collection software was provided by OLIS, and data fitting was performed with ORIGIN (Microcal, Inc.) software. For temperature control, coolant provided by a Neslab RTE 110 controller was flowed through the thermojacket surrounding the storage syringes and flow cell, and the temperature was monitored by a thermocouple mounted on the mixer. Stopped-flow measurements of Nir activity were done under anaerobic conditions. Solutions were initially argon-flushed, and to eliminate dissolved oxygen, we used a "cocktail" of glucose oxidase (0.1 mg/mL), catalase (0.1 mg/mL), and glucose (12 mM) in the reaction mixture with a 25 min wait for oxygen to be consumed after being loaded in the stopped-flow syringes. For most experiments, iso-1-ferrocyt *c* in one syringe at a 50 μM concentration, chosen so as not to be rate-limiting, was mixed with 5 μM Nir and 500 μM nitrite in the other syringe. The nitrite concentration which was above the K_m for nitrite (*5*) was also chosen not to be rate-limiting. Oxidation of iso-1-ferrocyt *c* was monitored in the Aminco-Morrow stopped-flow attachment. The number of reducing equivalents consumed was determined by the relation $\Delta\epsilon_{(\mathrm{Red-Ox})550} = 2.1 \times 10^4\ \mathrm{M}^{-1}\ \mathrm{cm}^{-1}$ (*26*). For monitoring deuterium isotope effects, we used D_2O (99.9%, Cambridge Isotope Laboratories); the pD of the reaction mixture was adjusted according to the relation $\mathrm{pD} = \mathrm{pH}_{\mathrm{meter}} + 0.4$ (*27*).

Spectroscopic Methods. Optical spectra were recorded with a Shimadzu dual beam spectrophotometer (slit width = 1.0). X-band EPR was carried out with a ER-200 IBM Bruker X-band spectrometer equipped with a standard rectangular TE_{102} X-band EPR cavity and an APD Cryogenics LTR-3 Helitran system (Allentown, PA). EPR data were collected in a Compaq computer using the EW Software routines (Scientific Software Sales). Q-band (34 GHz) ENDOR measurements were performed at 1.9 K under dispersion (χ'), rapid-passage field-modulated conditions with a cryogenically tunable TE_{011} Q-band resonator (*28*) as previously reported by Veselov et al. (*6*).

Proton ENDOR Analysis. Proton ENDOR frequencies, $^{\mathrm{H}}\nu_{\mathrm{ENDOR}}$, center to first order at the proton Larmor frequency, ν_{H} (>44 MHz for fields used at Q-band), and split away from the proton Larmor frequency by $\pm 1/2A$, where A is

the hyperfine coupling. Thus, the ENDOR frequencies are ${}^{H}\nu_{ENDOR}{}^{\pm} = |\nu_H \pm A/2|$, and under rapid-passage conditions, the intensity of the two branches $\pm$ need not be the same (*29*). For a number of the exchangeable proton features, the ${}^{H}\nu_{ENDOR}{}^{-}$ branch, whose frequency is given by $|\nu_H - A/2|$, was better resolved.

For exchangeable protons which experience dipolar couplings, a series of ENDOR measurements versus *g* value was used to obtain an estimate of distance from the proton to copper and the orientation of the principal dipolar axis with respect to the $g_{||}$ direction. Detailed simulations and overlay of predicted ENDOR frequencies with proton ENDOR spectra are provided in Figures 4S, 5S, 6S, and 7S in the Supporting Information. As pointed out in Veselov et al. (*6*), the dipolar coupling of such protons, A_D, is given by

$$A_D = \{f_{Cu} g_e g_n \beta_e \beta_n / hR^3\}(3\cos^2\omega - 1) = A_{dip}(3\cos^2\omega - 1) \quad (2)$$

where f_{Cu} is the fraction of an unpaired electron on the copper (in the range 0.8−1.0), g_e is the electronic *g*-value, and g_n is the nuclear *g*-value (=5.585 for a proton). *R* is the copper−proton distance, and ω is the angle between the vector **R** and the external magnetic field. The overall dipolar Hamiltonian will be axial with respect to the **R** direction. The principal axis of dipolar coupling need not be collinear with the **g**-tensor axes, and in frozen solution, angle selection determines the position and resolution of ENDOR features when they are displayed as a function of the magnetic field or *g*-value where taken. Hoffman and Gurbiel (*30*) devised a formulation for rapidly simulating polycrystalline ENDOR frequency patterns of systems such as Type 2 copper which have an axial **g**-tensor and a large axial copper ($^{63}Cu/^{65}Cu$) nuclear hyperfine coupling. This formulation does not depend on detailed simulation of ENDOR line shapes, and from the behavior of the outlying ENDOR features as a function of *g*-value, one can infer the magnitude of A_{dip} (and therefore *R*) and the angular orientation (β) of the proton with respect to the $g_{||}$ axis. [See pp 6103−6104 of Veselov et al. (*6*) for a more complete explanation.] β is the angle between **R** and the $g_{||}$ axis and is not generally the same angle as ω, which is the angle between **R** and the external magnetic field. As shown in the Supporting Information, there will be subsets of spectra corresponding to each copper nuclear spin state, $M_I = 3/2, 1/2, -1/2, -3/2$. The *g*-value range over which the maximal hyperfine coupling $A_D = 2A_{dip}$ is observed depends on the value of β, and if $\beta \neq 0$, the maximum proton hyperfine splitting with best resolution will be less than $2A_{dip}$ and will not be observed at the maximal *g*-value.

RESULTS

Kinetic Characterization

Optical and EPR spectra from wild-type, M182T, and H287E Nir have previously been reported (*5*). The optical spectra (Figure 2S and Table 1S, Supporting Information) of the other mutants studied here (D129A, D129N, H287A, I289A, and I289V) were similar to those of the blue−green wild-type enzyme with comparable intensity at 589 and 457 nm. In Figure 2 a comparison is provided of the X-band EPR spectra of wild-type enzyme with the new mutants D129A, D129N, H287A, I289A, and I289V used in this study. I289V, which is the most active of the mutants studied,

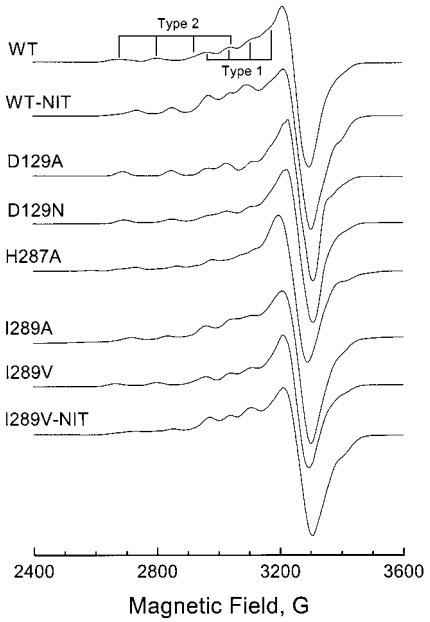

FIGURE 2: EPR spectra of forms of Nir studied in this work: WT (wild type), WT + nitrite, D129A, D129N, H287A, I289A, I289V, I289V + nitrite. These spectra were taken from samples at pH 7.5 in 0.05 M HEPES. X-band EPR spectra were obtained at $T = 15$ K, $\nu_e = 9.51$ GHz, 100 kHz modulation = 10 G ptp, 2 mW power. Enzymes were approximately 0.5 mM in total copper.

showed a change in its Type 2 features on addition of nitrite as has wild-type enzyme (*5*). The ratio of the Type 2 $g_{||}$ copper EPR features at low field to the combined Type 1 and Type 2 features near $g_\perp$ showed a significant complement of Type 2 copper for the Asp129 and His287 mutants. The amount of copper per subunit was analytically determined by a combination of protein analysis and biquinoline assay as 2.0 coppers per subunit for wild-type Nir and the I289A and I289V mutants and as approximately 1.5 coppers per subunit for the Asp129 and His287 mutants (Table 2S, Supporting Information). Based on the extinction coefficient for Type 1 copper (*5*), the D129A, D129N, and H287A mutants have 0.5−0.7 Type 2 copper, which is less than a complete Type 2 complement per subunit but not enough diminution of Type 2 copper to account for the loss of activity of the D129A, D129N, and H287A mutants.

The methyl viologen assay provided semiquantitative evidence of the different activities of our mutant enzyme (Supporting Information, Figure 3S); it identified the greater than 2 orders of magnitude loss of activity of the H287A mutant and indicated that D129A&N mutants had lost at least an order of magnitude in activity. Figure 3 shows the rapid stopped-flow iso-1-ferrocyt *c* consumption brought on by wild-type enzyme and the M182T, I289V, and I289A mutants; the much slower progress in consumption for the D129A mutant is indicated by a much longer time scale in the inset. The His287 mutations [H287A and previously H287E (*5*)] reduced the activity so much that it was not possible to distinguish their activity from the low background of iso-1-ferrocyt *c* oxidation in the absence of nitrite reductase; thus, the methyl viologen assay was needed to establish the extremely low activity of His287 mutants.

We quantitatively determined the initial rate of iso-1-ferrocyt *c* oxidation from the stopped-flow profile, where this consumption was brought on by 2.5 μM Nir. For wild-

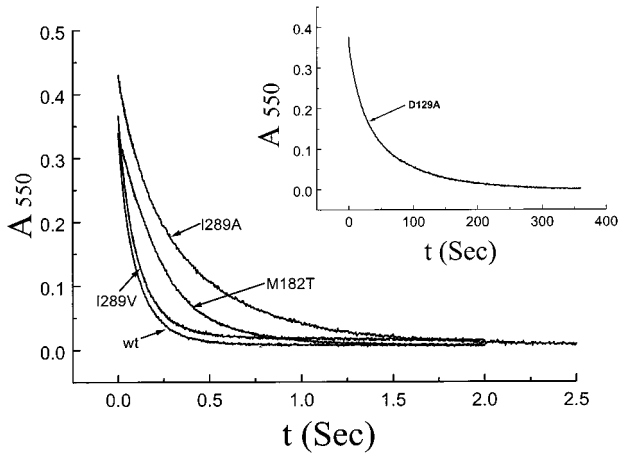

FIGURE 3: This figure compares the progress curves for iso-1-ferrocyt *c* consumption due to equal (2.5 μM) concentrations of the following enzyme forms: wild type, M182T, I289V, I289A, and D129A. (Note the much slower time scale in the inset for D129A.) All studies were carried out at pH 6.0 in the initial presence after mixing of 25 μM iso-1-ferrocyt *c* and 0.25 mM nitrite.

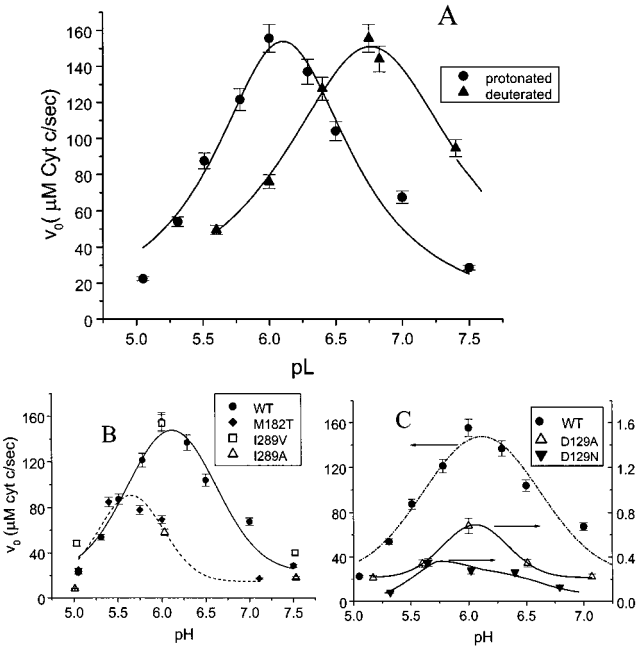

FIGURE 4: (A) The figure shows the profile for the initial rate of iso-1-ferrocyt *c* oxidation due to wild-type nitrite reductase as a function of pL, i.e., pH in H_2O and pD in D_2O. (B) This figure compares the rate profile as a function of pH for the more active variants which are wild-type enzyme, M182T, I289V, I289A. (C) This figure compares the rate profiles as a function of pH of wild-type enzyme to the less active D129A and D129N, whose turnover is very slow, as indicated by the right vertical axis.

type enzyme, the pH profile of the initial rate (in micromolar iso-1-ferrocyt *c* consumed per 2.5 micromolar of Nir per second) is shown in Figure 4A. There was a bell-shaped pH profile to this rate that peaked near pH 6. Since protons are transferred in the stoichiometric equation (eq 1) for nitrite reduction in a pH-dependent process, we sought explicit evidence for involvement of protons in the rate-limiting catalytic event by probing for a solvent deuterium isotope effect. We present the resultant pD profile of the nitrite reduction by wild-type enzyme in Figure 4A, where the "pL" notation (*27*) refers to pH in protonated solvent and pD in deuterated solvent. The presence of deuterium shifts the

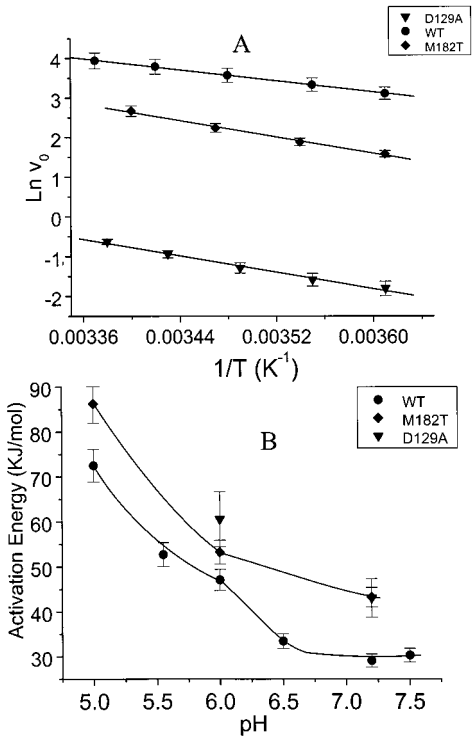

FIGURE 5: (A) This is a comparison of Arrhenius plots (rate vs reciprocal of absolute temperature) for wild-type enzyme, M182T, and D129A at pH 7.2. The activation energies were respectively 29, 43, and 43 kJ/mol. (B) This figure shows the activation energy for wild-type and M182T and D129A enzymes as a function of pH.

activity curve but not its maximum rate. We next compared the pH dependences of the initial rate for mutants in Figure 4B,C. As shown in Figure 4B, the mutation I289V altered the activity very little, and the mutation I289A reduced the activity about 3-fold. The activity of the M182T mutant was comparable to that of wild-type enzyme although there was a shift in its pH dependence. As shown in Figure 4C, the D129A and D129N mutations reduced the activity by a factor of ~100, and the pH dependence of D129N was altered although D129A appeared to retain a pH maximum near 6.

Our next object was to determine the explicit involvement of the Type 1 site in the rate-limiting step by observing the perturbation to activation energy arising from the M182T mutation at that site. The activation energies were measured from the temperature dependence of the initial rate of enzyme turnover, and the inset to Figure 5A shows Arrhenius plots of rate versus temperature as determined at pH 7.2 where redox potential measurements had previously been done (*5*). Over the range of temperature covered from 5 to 30 °C, the rate for wild-type enzyme was consistently 3−4 times larger than for M182T, and the slope of the Arrhenius trace less. The activation energies for wild type, M182T, and D129A at pH 7.2 were respectively 29, 43, and 43 (±6) kJ/mol. The plots of activation energy versus pH for wild-type enzyme, M182T, and D129A in Figure 5B indicate that the M182T mutation of the Type 1 center increased the activation energy throughout the pH range studied. The D129A and D129N mutations also increased the activation energy of wild type. Wild-type Nir, M182T, and D129A all showed a common increase in activation energy as the pH decreased below pH 6.5. Values of activation enthalpy and entropy obtained via Eyring plots are compared in the Supporting Information

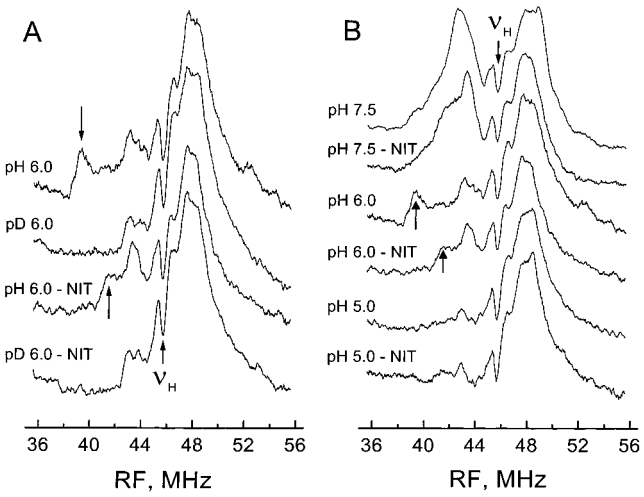

FIGURE 6: Panel A shows evidence for a particularly strongly coupled exchangeable proton feature from wild-type Nir in the absence and presence of nitrite (6 mM) where the best resolved feature is the $^{H}\nu_{ENDOR}^{-}$ feature below ν_H. For those spectra labeled NIT, the nitrite concentration was 6 mM. The exchangeable proton indicated by the arrow in the absence of nitrite has a coupling of 12.7 MHz while for that in the presence of nitrite the coupling is 9.0 MHz. Panel B provides evidence for the change in the strongly coupled proton features as a function of pH (pH 7.5 in 0.05 M HEPES, pH 6.0 in 50 mM MES, and pH 5.0 in 0.05 M sodium acetate) and the presence and absence of nitrite. Conditions were as follows: microwave power = 0.24 μW, field modulation 5 G, RF power about 20 W pulsed with 10% duty cycle, ν_e = 34.08 GHz, H = 1.068 T, g = 2.280, frequency sweep rate 2 MHz/s, and each spectrum was the average of 200 traces, each taking 10 s.

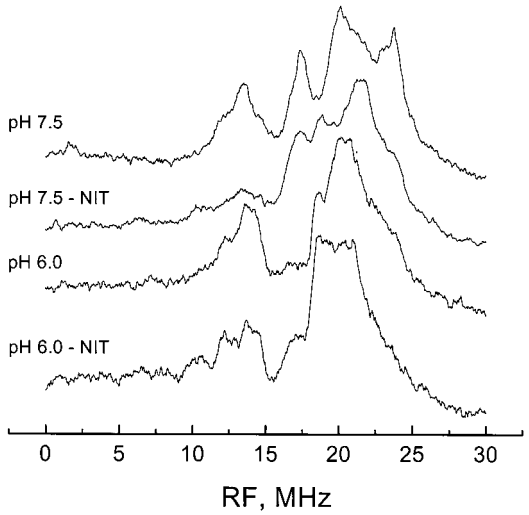

FIGURE 7: This figure from wild-type Nir shows a comparison of histidine nitrogen hyperfine features at pH 7.5 where the enzyme is not particularly active and at pH 6.0 where it is active. Spectra were taken both in the presence of 6 mM nitrite (indicated by "NIT") and in the absence of it. ENDOR conditions were as follows: microwave power = 0.80 μW, field modulation 2 G, RF power about 20 W pulsed, ν_e = 34.09 GHz, H = 1.038 T, g = 2.35, frequency sweep rate 6 MHz/s, and each spectrum was the average of 400−1600 traces, each taking 5 s.

(Table 3S) for wild-type enzyme at pHs in the 5.0−7.5 range and in Table 4S for wild-type, M128T, D129A, and D129N at pH 7.2. For wild-type enzyme, the positive activation enthalpy increased below pH 6.5 while the already negative activation entropy became increasingly more negative above pH 6.0; the activation free energy was at a minimum near pH 6.0 where the rate of nitrite reduction is maximal.

ENDOR Results

ENDOR Results from Wild-Type Nir: The pH Dependence. ENDOR supplied intimate and definitive evidence for proton and proton-related electronic effects to correlate with the pH dependence of Nir activity. A larger field modulation of 5 G ptp for rapid-passage ENDOR (*6*) was notably effective in resolving the large exchangeable proton coupling from the outlying $^{H}\nu_{ENDOR}^{-}$ branch (indicated by arrows) from which the proton features are shown in Figure 6. Figure 6A, taken at pH 6.0 where the activity is largest, shows the outlying exchangeable proton feature which responds to nitrite as well as pH. The coupling of the arrowed exchangeable feature was 12.7 ± 0.5 MHz in the absence of nitrite substrate, while in the presence of nitrite the largest coupling was found to be 9.0 ± 0.5 MHz. Figure 6B reveals the marked change in outlying proton features as a function of pH and the presence of substrate. At pH 7.5, the proton hyperfine pattern has an intense pair of features with a coupling of about 6 MHz, which we had previously noted at pH 7.2 to have an exchangeable component (*6*). The feature at pH 7.5 was altered by the presence of nitrite substrate. At pH 5.0, the strongly coupled proton features have largely disappeared, both with and without nitrite. The exchangeable features at pH 6 were followed as far as practical in the range g = 2.35−2.22 (Supporting Information, Figures 5S and 7S) before overlap of them with features of the Type 1 center occurred. Although the 2.35−2.22 range of g-values was insufficient to obtain a good angle-selected pattern, we determined that the best resolution and maximal splitting of the proton features occurred at about g = 2.28 in the absence of substrate and 2.24 in the presence of substrate, rather than at the highest g-value as might be expected if the $\mathbf{g}_{||}$ tensor and the maximal principal hyperfine axis for these protons were collinear. Figure 7 shows that the histidine nitrogen ENDOR features varied with pH in the presence and absence of nitrite. At pH 6 and in the presence of nitrite, the histidine nitrogen couplings overall diminished.

ENDOR of Mutant Nir. We next turned to mutants of the conserved protonatable groups His287 and Asp129, which had vastly diminished activity, to determine if there was substantial alteration of their proton ENDOR signals. In Figure 8 we provide a comparison of wild-type enzyme and the mutants H287A, D129A, and D129N whose features are shown from enzyme at pH 6.0. For H287A (pH 6.0), there remained the protons with a coupling of about 6 MHz similar to those observed from wild-type enzyme at pH 7.5, whose spectrum at pH 7.5 is provided in Figure 8 for comparison to H287A. The proton features of D129N, though present, were considerably less distinct than those of wild-type Nir, and they were not altered by addition of nitrite. There was no evidence for a strongly coupled exchangeable proton for D129A (pH 6.0), whose spectrum was similar to that of wild-type Nir at pH 5.0.

The I289A&V mutants had enzymatic activity comparable to that of wild-type enzyme; however, ENDOR revealed differences in their ligand binding site. We show in Figure 9 a comparison between wild-type enzyme, I289V, and

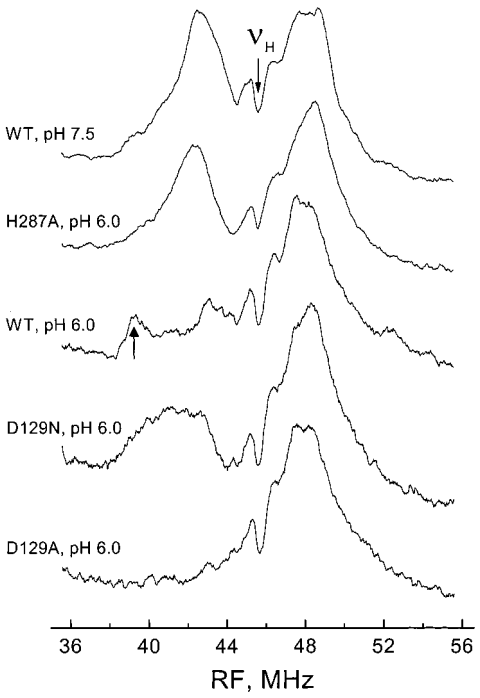

FIGURE 8: This figure compares the evidence for perturbation to the strongly coupled proton feature observed for wild-type Nir as brought on by the H287A, D129A, D129N mutations. The spectra shown are from wild type (WT) at pH 7.5 compared to H287A (pH 6.0) and wild-type enzyme (pH 6.0) compared to D129A (pH 6.0) and D129N (pH 6.0). The strongly coupled exchangeable proton noted at pH 6.0 (Figure 6) is indicated by an arrow. Conditions for ENDOR were as in Figure 6.

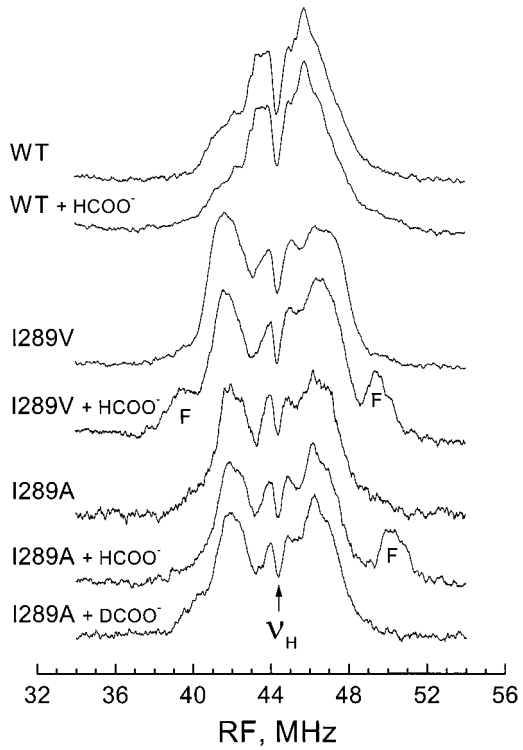

FIGURE 9: The spectra show a comparison of wild-type enzyme, I289A, and I289V in the absence and presence of 0.5 mM sodium formate ($HCOO^-$). The proton feature labeled F is from the formate. The spectrum of I289A prepared with 2 mM deuterated formate ($DCOO^-$) shows that the feature labeled F arises from the proton on formate. The pH was 6.0 for all samples. ENDOR conditions were as follows: microwave power = 0.24 μW, field modulation 1 G, RF power about 20 W pulsed with 10% duty cycle, ν_e = 34.08 GHz, H = 1.038 T, g = 2.35, frequency sweep rate 2 MHz/s, and most spectra were the average of 200 traces, each taking 10 s. The spectrum of I289A and the spectrum of I289A with formate respectively took 600 and 800 traces.

I289A obtained in the presence of 0.5 mM formate, a molecule similar in shape and charge to nitrite. For the I289V and I289A mutants, there was a notable new proton feature arising from the formate. The I289A mutant prepared with 2.0 mM deuterated formate (labeled $DCOO^-$ as opposed to $HCOO^-$) showed by absence of this formate-induced proton feature that the new feature was from the nonexchangeable proton on the formate.

Cysteine ENDOR of the Type 1 Site: Its Sensitivity to pH Change and Asp129 Mutation at the Type 2 Site. We have already shown the kinetic involvement of the Type 1 center in the rate-limiting electron-transfer step, and so we probed the effect of pH on the strongly coupled cysteine C_β proton ENDOR. This particular ENDOR signal is well resolved at g = 2.03 (H = 1.200 T), where there is no possibility of its more strongly coupled features being overlapped with features of the Type 2 site. The overall proton spectrum from the Type 1 copper is shown in the inset to Figure 10, and the explicit $^H\nu^+$ cysteine C_β proton feature, which has a large coupling of ~22 MHz, was followed in detail. On taking wild-type Nir from high pH (Figure 10a,b) to pH 6.0 (Figure 10e,f) to pH 5.0 (Figure 10g) either in the presence or in the absence of nitrite, there was an increase in the splitting of the cysteine C_β proton feature which accounts for an increase of about 1.5 MHz in the hyperfine coupling from 21.6 to 23.1 MHz. The mutation of Asp129, which is closer to Type 2 copper than to Type 1 copper, appeared to eliminate this pH-dependent perturbation. The D129A mutant (Figure 10c,d) happened to retain the smaller coupling of about 21.6 MHz, and D129N (Figure 10h,i) happened to retain the larger coupling of about 23.1 MHz.

DISCUSSION

Kinetic Characterization

pH/pD Profile of Enzymatic Activity. The pH dependence of the wild-type enzyme (Figure 4A), as measured by the initial rate of iso-1-ferrocyt *c* consumption, resembles the pH dependence measured from k_{cat} determined by steady-state turnover of Nir in the presence of highly reducing viologen systems (*9*, *10*, *31*). Such a maximum in the activity predicts near the active site a deprotonated species (e.g., Asp) with a pK_A near 5 and a protonated species (e.g., His) with a pK_A near 7 (*12*, *32*). Interestingly, pulse radiolysis experiments which create highly reducing species have also indicated a similar pH maximum to electron-transfer events from the Type 1 center, as monitored optically, in the presence of nitrite (*11*, *33*). pH dependence definitely points to the involvement of protons. If proton transfer or concerted proton-coupled electron transfer were to be part of the pH-dependent rate-limiting nitrite reduction process, then there should be a kinetic deuterium isotope effect. The presence of deuterium horizontally shifts the rate profile curve of Figure 4A, but it does not change the maximum rate. This horizontal shift in the profile indicates deuterium-induced shifts in pK_A values of protonatable groups [see Figure 1 of (*27*) for explanation]. The charges of the protonatable groups in this case would alter the rate-limiting step but would not

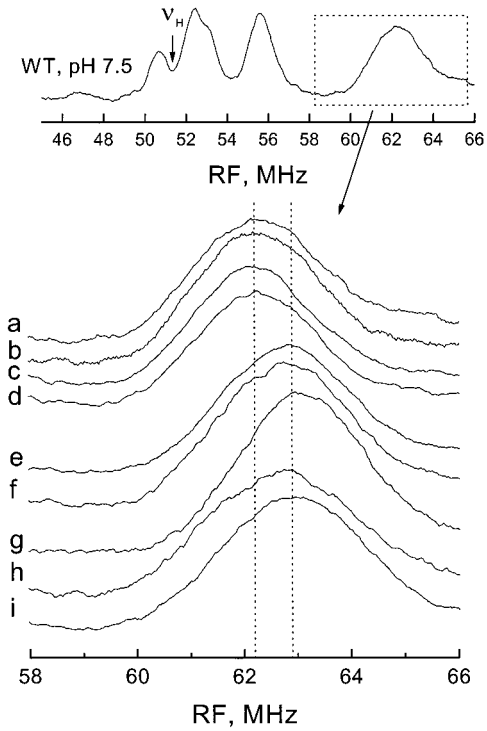

FIGURE 10: These spectra show the ~1 MHz increase of the strongly coupled cysteine C_β proton ENDOR feature near 62 MHz from the Type 1 center. The increase was brought on by changing the pH from 7.5 to 6.0. This change in frequency corresponds to a change in the proton hyperfine coupling itself from 21.6 to 23.1 MHz. The inset at the top shows the overall cysteine C_β proton spectrum. Mutation to Asp129 eliminated this change of proton coupling with pH, where the D129A mutant retained the smaller coupling and D129N retained the larger coupling. Spectra are as follows: a, WT-pH 7.5; b, WT-pH 7.5 + NIT; c, D129A-pH 7.5; d, D129A-pH 6.0; e, WT-pH 6.0; f, WT-pH 6.0 + NIT; g, WT-pH 5.0; h, D129N-pH 7.5; i, D129N-pH 6.0. ENDOR conditions were as follows: $T = 1.9$ K, microwave power = 0.24 μW, modulation 2 G, RF power about 20 W pulsed with 10% duty cycle, ν_e = 34.08 GHz, $H = 1.200$ T, $g = 2.03$, frequency sweep rate 3 MHz/s, and each spectrum was the average of about 50 traces, each taking 10 s.

themselves be involved in proton transfer during the rate-limiting step, although protons may be transferred before or after that rate-limiting step. For the wild-type enzyme, such proton(s) may be already appropriately positioned for catalysis, and detection of their position near the copper is a major goal of our ENDOR study.

Separate mutation of the two protonatable groups, Asp98 and His255, led to a vast diminishment in Nir activity, elimination of its pH maximum, and a diminished capacity for nitrite binding (*10, 12*). Our observation with homologous Asp129 and His287 mutants of *R. sphaeroides* indicates a similar loss of activity and of the pH dependence to that activity. The local charge environment at the Type 2 center appears to be affected by protonatable groups of Asp and His whose pK_A's are probably the pK_A's shifted by deuteration. Although Ile289 is a conserved side chain, the mutations I289A and I289V, which are unlikely to alter the local charge environment, showed no profound alteration of Nir activity.

Activation Energy and Electron Transfer. The next goal was to probe the electron-transfer nature of the rate-limiting step, for which activation energy measurements proved illuminating. Pulse radiolysis experiments utilizing extremely reducing species have indicated electron transfer from the

Table 1: Structural Information from Exchangeable Proton ENDOR Wild-Type Nir

axial ligand, pH	proton hyperfine coupling, $A_{\|\|}$ (MHz)	estimate of Cu−proton distance (Å)[a]	estimate of angle (deg) between $g_{\|\|}$ and $A_{\|\|}$
OH_X, pH 6.0[b]	12.7 ± 0.5	2.25−2.45	30 ± 10[c]
NO_2^-, pH 6.0[b]	9.0 ± 0.5	2.50−2.75	30 ± 10[c]

[a] The smaller distance is obtained from eq 2 with f_{Cu}, the spin density on the copper, taken as 0.8, and the larger distance is obtained from eq 2 with $f_{Cu} = 1.0$. [b] From Figure 6. [c] Estimated from angle-selected ENDOR theory which correlates the *g*-value where maximal splitting and best resolution of proton coupling occurs with the angle between $g_{\|\|}$ and the principal proton hyperfine axis.

Type 1 center in the presence of a functional Type 2 center (*11, 34−36*) both with and without nitrite. Our approach to determine the involvement of the Type 1 center was to use a cytochrome reductant with a physiologically appropriate redox potential and to confirm the involvement of the Type 1 center by perturbation to activation energy from the M182T mutation of that center. This mutation perturbed enzymatic activity but in no sense eliminated a functional Type 1 center as had, for example, a Met-to-Glu mutation at the Type 1 center (*37*). The M182T mutation alters the redox potential (i.e., driving force) (*5*) and conceivably the reorganization energy (*38*) for electron transfer. The different activation energy for Nir activity of M182T at all pHs implied the involvement of the Type 1 center in the rate-limiting step, a confirmation that the rate-limiting step is electron transfer from the Type 1 center to the nitrite-bound Type 2 center. The D129A (Figure 5) and D129N mutations (Table 4S) also altered the activation energy. The implication is that Asp129, with its protonatable and potentially hydrogen-bonding carboxylate adjacent to the nitrite binding site, sets the stage for optimal electron transfer *to nitrite*. We note that the work of Zhang et al. (*39*) demonstrated a role for the *A. faecalis* homologue of Asp129 in controlling the orientation and dynamics of CO ligand binding to the reduced Type 2 copper center. There is a common underlying increase in activation energy at pHs below pH 6.5 for wild-type, M182T, and Asp129 mutants, and we are not certain of the cause for this common increase.

Correlating ENDOR Evidence with Enzyme Function

At pH 6.0, where wild-type Nir is most active, the ENDOR evidence is for a strongly coupled exchangeable proton whose coupling is 12.7 MHz in the absence of nitrite and 9.0 MHz in the presence of nitrite. Simultaneously with the pH-induced change in enzyme activity, the existence and coupling of these proton features most obviously changed. If these couplings correspond to the largest principal value of a dipolar hyperfine coupling, then with a spin density on the copper in the range 0.8−1.0 (see eq 2 and Table 1) the respective distances of the observed proton from the Type 2 copper would be 2.25−2.45 Å in the absence of nitrite and 2.50−2.75 Å in the presence of nitrite. The proton couplings for these features were followed over a limited *g*-value range from 2.35 to 2.22 as shown in Figures 5S and 7S (Supporting Information); the reason for the limitation is the overlap at lower *g*-values with the Type 1 ENDOR features. In the presence of nitrite, the maximal value of coupling and best resolution occurred at $g = 2.24$ (Figure 7S), and in the

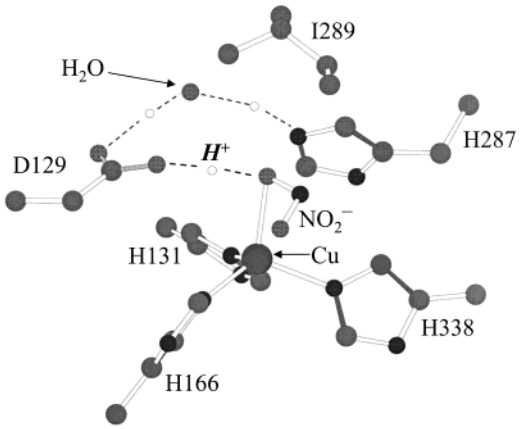

FIGURE 11: The schematic shows the Type 2 center in the presence of nitrite ligand as determined from the X-ray work of Murphy et al. (PDB file 1AS6) (*4*). The bridging water oxygen between His287 and Asp129 is shown, and additional protons (not directly located by X-ray crystallography) are indicated in the hydrogen-bonding network stretching from His287 to Asp129. Here the closer oxygen of nitrite is shown to be hydrogen bonded to the carboxylate oxygen (OD1) of the Asp129 ligand via the critical proton labeled with a script *H*.

absence of nitrite, the maximal value of coupling and best resolution occurred at $g = 2.28$ (Figure 5S). Although it would take single-crystal EPR to correlate $g_{||}$ with molecular coordinates, $g_{||}$ is usually found near the copper-to-axial ligand bond. The evidence was definite that the proton-to-copper vector was not collinear with $g_{||}$ because, if it were collinear, the maximum splitting and best resolution would have occurred near $g = 2.35$. Approximate angle selected theory (*6, 30*) detailed in the Supporting Information (Figures 4S, 5S, 6S, 7S) indicates that the angle between $g_{||}$ and the principal hyperfine axis for these protons is $30 \pm 10°$, both in the presence and in the absence of nitrite. To correlate previous estimates of structure with estimates from ENDOR, we have examined the X-ray crystallographic evidence, and we show in Figure 11 a scheme of the local environs of the Type 2 center in the presence of nitrite after Murphy et al. (*4*). Besides the immediate histidine ligands to the Type 2 center, we include His287 and Asp129 and the intervening water between them (*4*), and we include the nitrite ligand which is asymmetrically bound by its oxygens to the copper. We have estimated the position of a notable proton predicted to reside in the hydrogen bond between the carboxylate oxygen (OD1) of Asp129 and the closest oxygen of the nitrite (*4, 12*). If we put this proton halfway between the OD1 of Asp129 and the nearest copper-ligating oxygen of nitrite, the distance from the copper to this proton would be 2.61 Å (compared with 2.50−2.75 Å estimated from ENDOR), and the proton−copper−nitrite oxygen angle would be 34°.[2]

The arrowed proton features shown in Figure 6 are definitely spectroscopic proton features which become most apparent at the pH when the enzyme is most active, and their estimated dipolar-determined distance from the copper is consistent with that of a proton hydrogen bonded to the substrate or, in the absence of substrate, to the axial OH_X ligand. The existence of these protons must be sensitive to the hydrogen-donating properties of the Asp129 carboxylate because their ENDOR signals were greatly perturbed by mutation of Asp129. Given the ENDOR evidence for proximity of these protons to copper and for their sensitivity to Asp129 mutation, it is likely that these protons are hydrogen bonded between Asp129 and the substrate nitrite oxygen or the OH_X ligand in the absence of nitrite, although there are other potential hydrogen-bonding protons near the ligand (*4, 12*). The existence of the hydrogen bond between the copper ligand and the Asp129 carboxylate has been inferred from X-ray crystallography (*4*), but its characteristic pH dependence has not been resolved by crystallography (*2*). The proton which is properly hydrogen bonded to nitrite at pH 6 is thought to be a critical player in Type 2 activity (*4, 12, 32*) because this proton appears to be positioned to provide a properly oriented oxygen−proton bond to enhance the formation of water once nitrite accepts a reducing electron. ENDOR resolves this proton. The histidine nitrogen ENDOR spectra point out that the exchangeable protons are not the only species altered at the Type 2 center by pH. The change in the ligating histidine nitrogen features indicates that the electron density at the ligands is altered with both pH and the presence of substrate; change in the local ligating structure is a factor that alters redox potential and reorganization energy.

At pH 7.5 where enzyme activity is less, there is evidence for a more weakly coupled, exchangeable proton with 6 MHz coupling; we have observed this proton previously at pH 7.2 and noted its axial orientation (*6*). A recent X-ray crystallographic study (*40*) at pH 8.5 has pointed to the existence of an OH_X ligand, plausibly an hydroxide, different from that at lower pH. From the change in the proton ENDOR, Figure 6B provides evidence that nitrite at a sufficiently high concentration will bind at or near the Type 2 copper at pH 7.5, but this binding of nitrite appears to be in a catalytically nonproductive mode that does not favor rapid nitrite reduction. The ENDOR from proton features of Nir in the presence of nitrite at pH 7.5 is different from that at pH 6.0. Loss of a proton from the imidazolium ring of His287 at high pH may open the axial ligation site to a changed configuration of solvent which alters the mode of axial ligand binding. It is also possible that the Asp129 carboxylate, coupled to the same imidazolium ring of His287 via the intervening water (see Figure 11), concomitantly alters its hydrogen-bonding capability when His287 loses its proton at high pH. It is of interest that loss of His287 by H287A mutation enhanced the species having the 6 MHz axial proton coupling even at lower pH values (pH 6.0 in Figure 8), again, plausibly, by opening the ligation site to a different configuration of solvent (*32*) or by inductively altering the properties of the Asp129 carboxylate.

The conservatively mutated I289V and I289A provided via their formate ENDOR spectra a possible reason for the importance of Ile289 in restricting the Type 2 ligand binding pocket. These mutants, in contrast to wild-type enzyme, allowed the formate to bind in the immediate vicinity of the Type 2 site, and, therefore, a purpose of the Ile289 may be to exclude unwanted ligands. Formate was for us a convenient choice of a molecule similar in size, charge, and shape to nitrite. It may be more important for the Type 2 center to

[2] We also performed a similar calculation for the structure in the absence of nitrite, and if we put a hydrogen-bonding proton halfway between the OD1 of Asp129 and the ligating oxygen of OH_X, the distance from the copper to this proton would be 2.18 Å, compared with 2.25−2.45 Å estimated from ENDOR, and the proton−copper−nitrite oxygen angle would be 43°.

exclude other small molecules such as hydrogen peroxide, oxygen, or superoxide, whose products are damaging to the enzyme and the cell. It is also of interest from a future protein engineering standpoint that mutating Ile289 has created a more promiscuous active site for binding of other ligands than nitrite.

The Type 1 center was shown here to be kinetically involved in the rate-limiting electron-transfer step. The cysteine β carbon is in the sigma bonding electron-transfer pathway from the Cys167 ligand of the Type 1 copper to the His166 ligand of the Type 2 copper (*36*). The hyperfine coupling reported by the cysteine Cys167 C_β proton is thus a reporter of the Cys167 electronic structure (*6*), and changing the pH provides evidence for a spin density change at the Cys167 or a conformational change of the Cys167. Additionally, the mutation of the Asp129 renders the Cys167 hyperfine couplings no longer sensitive to pH change, with the implication that this pH-dependent alteration of the Cys167 of Type 1 copper is transmitted through Asp129. Although most of our pH-related proton ENDOR spectroscopy has told of events at the Type 2 center, the pH dependence of the Cys167 C_β proton ENDOR may reflect the pH dependence of electronic coupling between Type 1 and Type 2 centers in the pathway for electron transfer.

ACKNOWLEDGMENT

We thank Dr. Kim A. DeWeerd for instruction in the megaprimer mutagenesis used in developing the I289A and I289V mutants and for sequencing of the resultant genes.

SUPPORTING INFORMATION AVAILABLE

Text is provided to explain in detail the methods by which mutants of Asp129, His287, and Ile289 were made. Table 1S lists optical properties of Nir mutants H287A, D129A, D129N, I289A, and I289V. Table 2S lists the copper content and ratio of Type 1 to Type 2 copper for wild-type Nir, M182T, H287A, D129A, D129N, I289A, and I289V. Table 3S provides activation energy, activation enthalpy, and activation entropy for wild-type Nir over the pH range 5−7.5. Table 4S tabulates activation energy, activation enthalpy, and activation entropy for wild-type Nir, M182T, D129A, and D129N at pH 7.2. Figure 1S is a sequence alignment of the Ile289 region of the copper-containing Nir from various bacteria. Figure 2S is the visible spectra of wild type, H287A, D129N, D129A, I289V, and I289A. Figure 3S compares relative activities of Nir as measured by the methyl viologen assay and provides text on this assay method. Figure 4S provides the detailed prediction of exchangeable proton ENDOR frequencies versus *g*-values from angle-selected theory (*30*) for the off-axis exchangeable proton with maximal dipolar coupling of 12.7 MHz in the absence of nitrite. Figure 5S provides spectra of the strongly coupled exchangeable proton ENDOR features versus *g*-value for Nir in the absence of nitrite at pH 6.0 and an overlay of the predicted proton frequencies for a proton with dipolar coupling of 12.7 MHz over a series of off-axis angles β between the copper-to-proton direction and the $g_{||}$ direction of 0°, 20°, 30°, and 40°. Figure 6S provides the detailed prediction of exchangeable proton ENDOR frequencies versus *g*-values from angle-selected theory (*30*) for an off-axis exchangeable proton with maximal dipolar coupling of 9.0 MHz in the presence of nitrite. Figure 7S provides spectra of the strongly coupled exchangeable proton ENDOR features versus *g*-value for Nir in the presence of nitrite at pH 6.0, and an overlay of the predicted proton frequencies for a proton with dipolar coupling of 9.0 MHz over a series of off-axis angles β of 0°, 20°, 30°, and 40°.

REFERENCES

1. Godden, J. W., Turley, S., Teller, D. C., Adman, E. T., Liu, M. Y., Payne, W. J., and LeGall, J. (1991) *Science 253*, 438−442.
2. Adman, E. T., Godden, J. W., and Turley, S. (1995) *J. Biol. Chem. 270*, 27458−27474.
3. Murphy, M. E. P., Turley, S., Kukimoto, M., Nishiyama, M., Horinouchi, S., Sasaki, H., Tanokura, M., and Adman, E. T. (1995) *Biochemistry 34*, 12107−12117.
4. Murphy, M. E. P., Turley, S., and Adman, E. T. (1997) *J. Biol. Chem. 272*, 28455−28460.
5. Olesen, K., Veselov, A., Zhao, Y., Wang, Y., Danner, B., Scholes, C. P., and Shapleigh, J. P. (1998) *Biochemistry 37*, 6086−6094.
6. Veselov, A., Olesen, K., Sienkiewicz, A., Shapleigh, J. P., and Scholes, C. P. (1998) *Biochemistry 37*, 6095−6105.
7. LaCroix, L. B., Shadle, S. E., Wang, Y., Averill, B. A., Hedman, B., Hodgson, K. O., and Solomon, E. I. (1996) *J. Am. Chem. Soc. 118*, 7755−7768.
8. Werst, M. M., Davoust, C. E., and Hoffman, B. M. (1991) *J. Am. Chem. Soc. 113*, 1533−1538.
9. Abraham, Z. H. L., Smith, B. E., Howes, B. D., Lowe, D. J., and Eady, R. R. (1997) *Biochem. J. 324*, 511−516.
10. Kataoka, K., Furusawa, H., Takagi, K., Yamaguchi, K., and Suzuki, S. (2000) *J. Biochem. (Tokyo) 127*, 345−350.
11. Kobayashi, K., Tagawa, S., Deligeer, and Suzuki, S. (1999) *J. Biochem. (Tokyo) 126*, 408−412.
12. Boulanger, M. J., Kukimoto, M., Nishiyama, M., Horinouchi, S., and Murphy, M. E. (2000) *J. Biol. Chem. 275*, 23957−23964.
13. Bradford, M. M. (1976) *Anal. Biochem. 72*, 248−254.
14. Hanna, P. M., Tamilarasan, R., and McMillin, D. R. (1988) *Biochem. J. 256*, 1001−1004.
15. Pollock, W. B. R., Rosell, F. I., Twitchett, M. B., Dumont, M. E., and Mauk, A. G. (1998) *Biochemistry 37*, 6124−6131.
16. Morar, A. S., Kakouras, D., Young, G. B., Boyd, J., and Pielak, G. J. (1999) *J. Biol. Inorg. Chem. 4*, 220−222.
17. Cutler, R. L., Pielak, G. J., Mauk, A. G., and Smith, M. (1987) *Protein Eng. 1*, 95−99.
18. DeWeerd, K., Grigoryants, V., Sun, Y., Fetrow, J. S., and Scholes, C. P. (2001) *Biochemistry 40*, 15846−15855.
19. Pielak, G. J., Auld, D. S., Beasley, J. R., Betz, S. F., Cohen, D. S., Doyle, D. F., Finger, S. A., Fredericks, Z. L., Hilgen-Willis, S., and Saunders, A. J. (1995) *Biochemistry 34*, 3268−3276.
20. Moore, G. R., and Pettigrew, G. W. (1990) *Cytochromes c Evolutionary, Structural and Physicochemical Aspects*, Springer-Verlag, Berlin.
21. Moore, G. R., Harris, D. E., Leitch, F. A., and Pettigrew, G. W. (1984) *Biochim. Biophys. Acta 764*, 331−342.
22. Berks, B. C., Ferguson, S. J., Moir, J. W. B., and Richardson, D. J. (1995) *Biochim. Biophys. Acta 1232*, 97−173.
23. Deligeer, Kataoka, K., Yamaguchi, K., and Suzuki, S. (2000) *Bull. Chem. Soc. Jpn. 73*, 1839−1840.
24. Tetreault, M., Rongey, S. H., Feher, G., and Okamura, M. Y. (2001) *Biochemistry 40*, 8452−8462.
25. MacGregor, C. H. (1978) *Methods Enzymol. 53*, 347−356.
26. Jensen, P., Aasa, R., and Malmström, B. G. (1981) *FEBS Lett. 125*, 161−164.
27. Schowen, K. B., and Schowen, R. L. (1982) *Methods Enzymol. 87*, 551−606.
28. Sienkiewicz, A., Smith, B. G., Veselov, A., and Scholes, C. P. (1996) *Rev. Sci. Instrum. 67*, 2134−2138.
29. Hoffman, B. M., DeRose, V. J., Doan, P. E., Gurbiel, R. J., Houseman, A. L. P., and Telser, J. (1993) in *Biological Magnetic Resonance, Vol. 13: EMR of Paramagnetic Molecules* (Berliner, L. J., and Reuben, J., Eds.) Plenum, New York.
30. Hoffman, B. M., and Gurbiel, R. J. (1989) *J. Magn. Reson. 82*, 309−317.
31. Kakutani, T., Watanabe, H., Arima, K., and Beppu, T. (1981) *J. Biochem. (Tokyo) 89*, 453−461.

32. Boulanger, M. J., and Murphy, M. E. (2001) *Biochemistry 40*, 9132−9141.
33. Suzuki, S., Kataoka, K., and Yamaguchi, K. (2000) *Acc. Chem. Res. 33*, 728−735.
34. Suzuki, S., Kohzuma, T., Deligeer, Yamaguchi, K., Nakamura, N., Shidara, S., Kobayashi, K., and Tagawa, S. (1994) *J. Am. Chem. Soc. 116*, 11145−11146.
35. Suzuki, S., Deligeer, Yamaguchi, K., Kataoka, K., Kobayashi, K., Tagawa, S., Kohzuma, T., Shidara, S., and Iwasaki, H. (1997) *J. Biol. Inorg. Chem. 2*, 265−274.
36. Farver, O., Eady, R. R., Abraham, Z. H., and Pecht, I. (1998) *FEBS Lett. 436*, 239−242.
37. Kukimoto, M., Nishiyama, M., Murphy, M. E. P., Turley, S., Adman, E. T., Horinouchi, S., and Beppu, T. (1994) *Biochemistry 33*, 5246−5252.
38. Marcus, R. A., and Sutin, N. (1985) *Biochim. Biophys. Acta 811*, 265−322.
39. Zhang, H., Boulanger, M. J., Mauk, A. G., and Murphy, M. E. P. (2000) *J. Phys. Chem. B 104*, 10738−10742.
40. Ellis, M. J., Dodd, F. E., Strange, R. W., Prudencio, M., Sawers, G., Eady, R. R., and Hasnain, S. S. (2001) *Acta Crystallogr., Sect. D: Biol. Crystallogr. 57*, 1110−1118.

BI0256274